Seasonal Dynamics of the Pantanal Ecosystem

Phase 1 Report

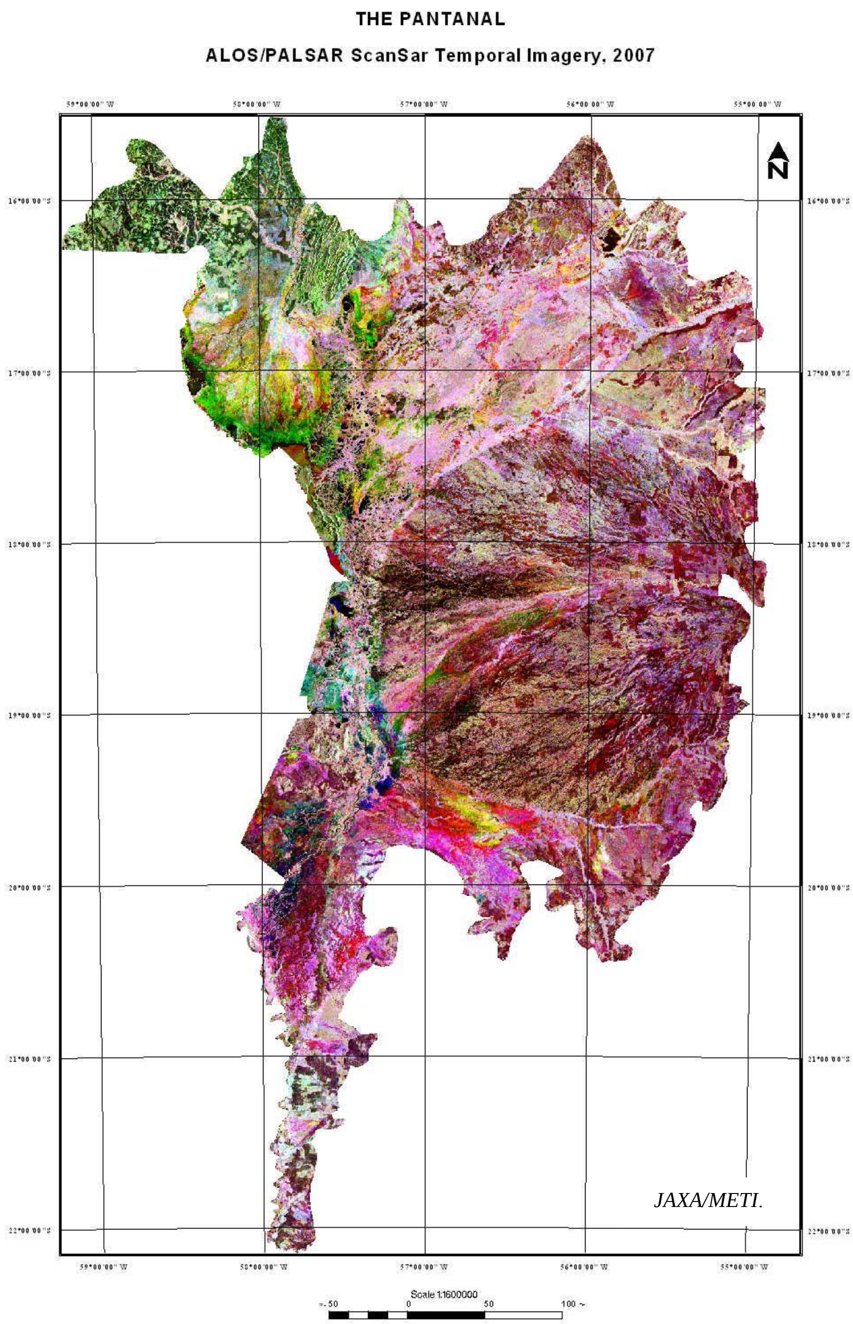

ALOS/PALSAR temporal data for 2007: Blue - February (rising water); Red - May (high water); Green - November (low water)

Seasonal Dynamics of the Pantanal Ecosystem

Maycira Costa[1] , Kevin Telmer[2] and Terresa Evans[1]
[1] Department of Geography; [2] School of Earth and Ocean Sciences, University of Victoria, 3800 Finnerty Rd., Victoria, BC Canada V8P 5C2
Email: maycira@office.geog.uvic.ca

***Abstract*—The Brazilian Pantanal is a large tropical wetland with an abundance of biodiversity and varied habitats. It is defined by a seasonal inundation pattern that varies both temporally and spatially. This study uses L-band ALOS PALSAR and C-band Radarsat-2 multi-temporal SAR data to map the seasonal ecosystems and the first spatial-temporal maps of the flood dynamics of the Pantanal. First, an understanding of the backscattering characteristics of flooded and non-flooded habitats was developed. Second, maps of habitats and flooding dynamics were generated using an object based classification method. A level 1 classification defining five cover types was achieved with accuracy results of approximately 77%. A level 2 classification separating flooded from non-flooded regions for five temporal periods over one year was also accomplished, showing large interannual variability between subregions in the Pantanal. Cross-sensor, multi-temporal SAR data was found to be useful in mapping both land cover and flood patterns in wetland areas. The generated maps will be a valuable asset for defining habitats required to sustain the Pantanal biodiversity and the impacts of human development in this region.**

***Index Terms*—ALOS PALSAR, K&C Initiative, Wetlands Theme, Pantanal, Conventions, Conservation, Flooding dynamics.**

I. INTRODUCTION

The Pantanal (Figure 1), the largest tropical wetland in the world, is roughly located in the center of South America, between Brazil, Bolivia, and Paraguay. In many ways, it is a unique landscape characterized by salt and freshwater lakes, abundant aquatic vegetation, and open and dense savanna (Pott, 2000, 1989; Abdon *et al.,* 1998; Costa and Telmer, 2006). It is fed by the upper Paraguay River and its tributaries (Figure 2) and these promote a strong annual flood. The degree of flooding and its duration and amplitude vary both yearly and spatially. The complicated flood dynamics makes the delimitation of the total area of the Pantanal extremely difficult (Por, 1995). Estimates suggest that the Brazilian Pantanal occupies an area that ranges from 138,000 km^2 during maximum flood (Silva and Abdon, 1998) to 11,000 km^2 during the dry season (Hamilton *et al.,* 1996), a difference of approximately 90%. The entire watershed of the Pantanal occupies an area of approximately 362,000 km^2.

Within the Pantanal, the occurrence of different habitats such as river corridors, gallery forests, perennial wetlands, and lakes (fresh and brackish lakes), seasonally flooded grass lands, and terrestrial forest is related to the dynamics of the flood cycle and its spatial variations. During the rising and maximum water stand, the dominant habitats are the large areas of floating and rooted aquatic vegetation, open water, and flooded forest. The flooded forest is mostly comprised of shrub-like trees and tall, densely foliated riparian trees (Silva and Abdon 1998). The aquatic vegetation is dominantly floating and rooted species that grow quickly during the maximum flood and die during the dry period. This dynamics of this wetland is the foundation for the many species of plants and animals – salviniaceaes, cyperaceaes, iguanas, tortoises, crocodiles, primates, and multitudes of fish, birds, and insects. However, it is the delicate interplay between the dynamic distribution of vegetation, the high biological productivity of the aquatic plants, the climate, and the hydrological cycle, that nourishes and sustains the incredible diversity of plants and animals. Unfortunately this interplay is poorly understood and is threatened by human development.

A series of human initiatives such as modification of the natural hydrological cycles of rivers, mining, agriculture, and chemical industry, construction initiatives (hydroelectric dams, dikes, Hydrovia, GASBOL – Bolivia-Brazil Gas pipeline), clearing of land and extensive burning, and commerce of wild animals are threatening this wetland ecosystem in an irreversible manner (Hamilton 1999; da Silva and Girard 2004). Some of the resultant effects are loss of habitat and biodiversity, water pollution (mostly mining byproducts and agrochemicals), and erosion and sedimentation of waterways (Gottgens et al. 1998). For example, the five governments of the La Plata basin, Brazil, Bolivia, Paraguay, Argentina, and Uruguay, have jointly developed plans to deepen the Paraguay River, canalize many meanders, and regulate inflows along its course from Cáceres, Brazil, to Porto de Nueva Palmira, Uruguay – an astounding 3400 km, the called Hydrovia (Paraguay-Parana Waterway Project). This project was designed aiming the cheaper transport of soy beans, oil, corn, cotton, manganese, and iron ore, at the expenses of one of the largest environmental disasters ever planned, the canalization and regulation of the Pantanal major rivers. This project as it was initially idealized was waned (recently it has been re-evaluated); however, various smaller hydrological initiatives remain of interest, which are accurate described by Gottens et al., 1998 as the “tyranny of small decisions”.

The state of this initiative is currently unclear, however, the Brazilian government has planned the construction of a series of small projects that when treated individually are considered too small-scale to warrant impact assessments, but that together represent potentially large scale change for the Pantanal (Gottgens 1998; da Silva and Girard 2004). The suspected consequences of these projects have been voiced by many critics – loss of wetlands, changes in water quality, reduction in the diversity of flora and fauna, and negative impacts on the livelihoods of local and indigenous people in the region. It is our hope to add to this debate and to do so provide a better understanding of the flooding dynamics of the Pantanal ecosystem. This document reports mostly the use of ScanSAR imagery for mapping the flooding dynamics; the use of fine resolution imagery requires more work on lakes classification (in progress). Also, fine resolution mosaics are not used in this report; at this time, we do not have access to these mosaics.

II. The Pantanal Project

A. Objectives and Relevance to the K&C drivers

As stated in the introduction, there is a lack of information on the spatial-temporal inundation pattern on the Pantanal. This is important information for understanding the biogeochemical cycles, the habitats required to sustain the Pantanal biodiversity, and the impacts of human development in the region. With this in mind, the objectives of this project were (1) to map the seasonal ecosystems and flood dynamics of the Pantanal and (2) to detail characterize lake types in the Pantanal. To attend the first objective, ScanSAR ALOS/Palsar and Radarsat 2 imagery were used to map variations in vegetation and monthly inundation extent during the year. To attend the second objective, ALOS/Palsar fine resolution imagery of a pilot area were used and fine resolution mosaics will be used when available.

Our objectives are clearly related to the Thematic drivers: **C**onventions, **C**arbon and **C**onservation, with a stronger focuses on the first and third, as we aim to map the flood dynamics that sustain the Pantanal wetland ecosystems.

B. Field data

Field data were acquired for 209 sites in the Brazilian Pantanal in July of 2008. Preliminary analysis of 2007 ALOS/PALSAR imagery, Landsat (provided in Google Earth Pro), and field data acquired in 2001 provided the approximate location of regions to be visited for this campaign. Three regions within the study area were chosen as pilot areas, comprised of the Nhecolandia, Aquidauana and Miranda subregions. Ground cover, as well as vegetation characteristics such as species and distribution were determined from direct observation, then recorded and photographed for each location; also 75 water samples for determining lakes geochemistry were sampled.

Figure 1. The Brazilian Pantanal displayed in grey. (GEF 2004).

C. Satellite data

The satellite dataset was acquired from two Synthetic Aperture Radar (SAR) systems: the Advanced Land Observing Satellite (ALOS) and RADARSAT-2. ALOS was launched in January 2006 by the Japanese Aerospace Exploration Agency, and carries onboard the variable-resolution and polarimetric Phased Array L-band Synthetic Aperture Radar (PALSAR) with a variety of spatial resolutions (Rosenqvist et al 2007). The PALSAR ScanSAR observation mode, used for this report, allows coverage of large areas of land. Radiometric accuracy of PALSAR products is reported as 1dB per scene (JAXA 2009). RADARSAT-2 was launched on December 2007 by the Canadian Space Agency, and also offers a variety of spatial resolutions and selective polarization.

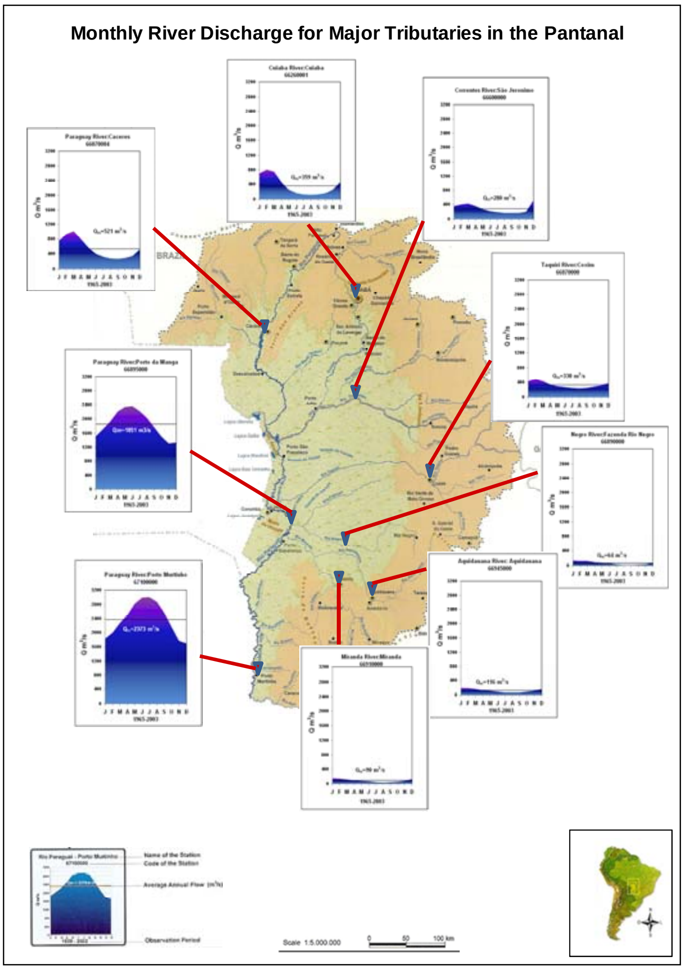

Figure 2. Monthly mean annual discharge for major tributaries in the Brazilian Pantanal. (Source: GEF 2004)

The acquired data set includes a temporal series of ALOS/PALSAR ScanSAR images from 2007, covering January, February, May, July, and November, and Radarsat-2 ScanSAR Narrow imagery from August of 2008. Each time period consists of a series of four contiguous images to be mosaicked together to provide complete coverage of the study area. The specific months of acquisition for the ALOS data were chosen due to the timing of the flood-pulse in the study region: January represents rising water; February high water; May receding; July nearly dry; and November fully dry (refer to Figure 2). The Radarsat-2 imagery was chosen as complementary information, corresponding to the timing of field data acquisition.

D. Imagery processing

Step 1: Raw data
ALOS raw image files were processed through the Alaskan SAR Facility's Map Ready software, using provided geometric and radiometric data. ALOS images were already calibrated for the antenna pattern and so were not subject to a Look-Up Table (LUT) scaling process. Radarsat-2 raw images were processed and orthorectified using PCI Orthoengine, using a SAR specific satellite orbiting model and 121 ground control points provided from MDA (MacDonald, Dettwiler and Associates Ltd.), the primary suppliers of Radarsat-2 imagery. The RADARSAT images were converted to original 32-bit format using a sigma-nought LUT (provided).

Step 2: Mosaicking
Each set of four images for each of the temporal periods was mosaicked together to form cohesive coverage of the entire Pantanal. Cutlines (the seams between individual images in a mosaic) were collected automatically based on minimum difference parameters with a blend width of three pixels. A vector file of the Pantanal floodplain provided by the Brazilian Agricultural Research Corporation (EMBRAPA) was then utilized to clip the study area from the mosaics.

Step 3: Geometry
To minimize possible geometric distortions a geometric correction approach based on ground control points collected in the images and a first order polynomial was applied. An RMS error of smaller than 1 pixel was deemed sufficient for this study. All of the images were examined visually for geometric inaccuracies: ALOS-ALOS same temporal period; ALOS-ALOS cross-temporal; RSAT-RSAT; and ALOS-RSAT. All images were projected to UTM coordinates (zone 21, row K) using the WSG84 reference ellipsoid.

There were no apparent geometric errors between ALOS images within the same time period. However, the February ALOS images displayed a slight shift in geometry compared to the other months, so a second order polynomial correction was performed using nine ground control points obtained from the January images. The RMS error for this correction was 0.31 for the x-axis and 0.51 for the y-axis. A comparison of the ALOS mosaics to the RSAT mosaics showed no significant geometric inconsistencies. However, when comparing Radarsat-2 images from 2 different satellite paths, there was a slight shift of 2 pixels in the x-axis between the western path and the eastern path. Because the error was consistent along the entire path, a simple shift of the west path to match the east executed the required correction.

Step 4: Preliminary Visual Interpretation
The series of mosaics was integrated into a single multi-layered dataset and visually examined for general patterns of ground cover. Colour composites using different temporal and cross-sensor combinations were created to aid in visual analysis and primary interpretation of the data (see example in Figure 3).

Step 5: Regions of Interest (ROI) Collection
ROI's were collected from the multi-layered mosaic, and were based on ground truth data, a priori knowledge of SAR backscattering characteristics, secondary information gathered from local inhabitants of the area, and examination of high

spatial resolution optical imagery (IKONOS and ANVIR-2). Table 1 outlines ROI categories, number of ROI per categories, and total number of pixels per category. Histograms for training sites were computed and the minimum, maximum, mean, and standard deviation for each was extracted.

Table 1. ROI categories.

Category	*Number of Training Sites*	*Total Number of Pixels*	*Class Description*
Savanna Forest	12	299	- does not flood; includes cordilhieras and capoes; 1-2m higher than terrain
Gallery/Floodable Forest	4	74	- gallery forest are riparian, occur on higher banks of major rivers; class also includes other seasonally flooded forest
Grasslands	6	39	- areas of natural grasslands
Floodable Grasslands	16	166	- areas of natural grasslands known to flood
Pasture	5	58	- cultivated, farmland and pasture
Floodable Pasture	4	35	- cultivated, farmland and pasture known to flood
Dense/Open Savanna	10	242	- herbaceous fields with shrubs and short trees
Floodable Dense/Open Savanna	3	30	- herbaceous fields with shrubs and short trees known to flood
Herbaceous Savanna	9	189	- occurs on sandy soils of alluvial fans, areas of herbaceous aquatic vegetation, vazantes and waterways
Open Water	4	327	- open water bodies; lakes and major rivers

Step 6: Backscattering Analysis
In order to understand the scattering processes of microwave radiation interaction with ground cover, as well as change in these scattering processes due to inundation, the backscattering values collected from the ROI were compared. For this comparison, the backscattering signal, minimum, maximum, and mean values of amplitude were then converted to normalized backscattering coefficients (σ^0) expressed in terms of dB. The conversion process from amplitude (DN) to backscattering in dB (σ^0) for ALOS/PALSAR is as follows:

$$\sigma^0 = 10*\log_{10}(DN^2)+CF$$

where CF is the calibration coefficient for PALSAR standard products, and equals –83 for the time of imagery acquisition and processing. (Rosenqvist et al, 2007).

Conversion of DN to σ^0 for Radarsat-2 ScanSAR images require a Look-up Table (LUT) which is included with the product, and the equation is as follows:

$$C = (DN^2 + B) / A$$

where C is the calibrated value; B is the offset (supplied in the LUT); and A is the range dependant gain (supplied in the LUT) (MDA, 2008). This step was performed during initial raw image processing in Orthoengine (PCI Geomatics). The calibrated values were then expressed in dB via the following calculation (Wessels, 2008 – personal communication):

$$dB = 10*\log(C)$$

Converted dB values were then examined visually to determine seasonal trends among classes, and any confusion between classes. After conversion of ALOS and RSAT minimum, maximum, and mean values from amplitude to dB backscattering, the values were analyzed for class specific and temporal changes.

Step 7: Speckle Filtering
For this study, three common adaptive filters were tested: Frost, Gamma and Kuan. Several tests were performed employing these three adaptive filters with a 3x3 and a 5x5 window, and using one, two and three interactions. Visual analysis of the resultant filtered images was performed to determine the best preservation of edge features and discrimination of different textured areas. After visually ruling out the 5x5 window, and the two and three interaction images, the remaining images were tested for mean backscattering preservation and decrease of standard deviation. Four samples (98, 183, 303 and 342 pixels) of a homogenous target (open water) were selected and the mean and standard deviation of each sample was calculated before and after filtering. The goal was to determine the method that best preserves the mean values, while decreasing the standard deviation (Oliver & Quegan 2004).

Once all of the mosaics were filtered, they were scaled to 8-bit images to reduce processing time during classification.

Step 8: Classification: Definiens Processing and Analysis
The classification scheme was organized in two levels aiming to capture different land cover types (Level 1) and seasonally flooded and non-flooded areas (Level 2).

Level 1 – Cover Classification
All 8-bit and amplitude ALOS image mosaics (January, February, May, July and November) as well as both 8-bit and amplitude Radarsat-2 images (August, HH and HV polarizations) were imported into Definiens. The 8-bit data was used for the segmentation processing, and the amplitude for defining the backscattering (dB) of the generated objects. The follow steps were performed:

A: Several combinations of the three multi-resolution segmentation parameters were tested in order to determine the optimal combination for this data. A scale factor of 20 resulted in object polygons that were refined enough to capture small objects such as the lakes as individual entities, without being so small as to confuse fuzzy borders. An emphasis on radiometry as opposed to shape was deemed important, therefore a factor of 0.3 was chosen as the best compromise, and the portion allotted to shape was divided evenly between smoothness and compactness as both were considered of equal importance. Only the February, the July, and the RSAT HV image were given weight for this segmentation as they were the layers deemed to have the most seasonal and spectral contrast (February being high water, July low water, and RSAT representing additional information from C-band).

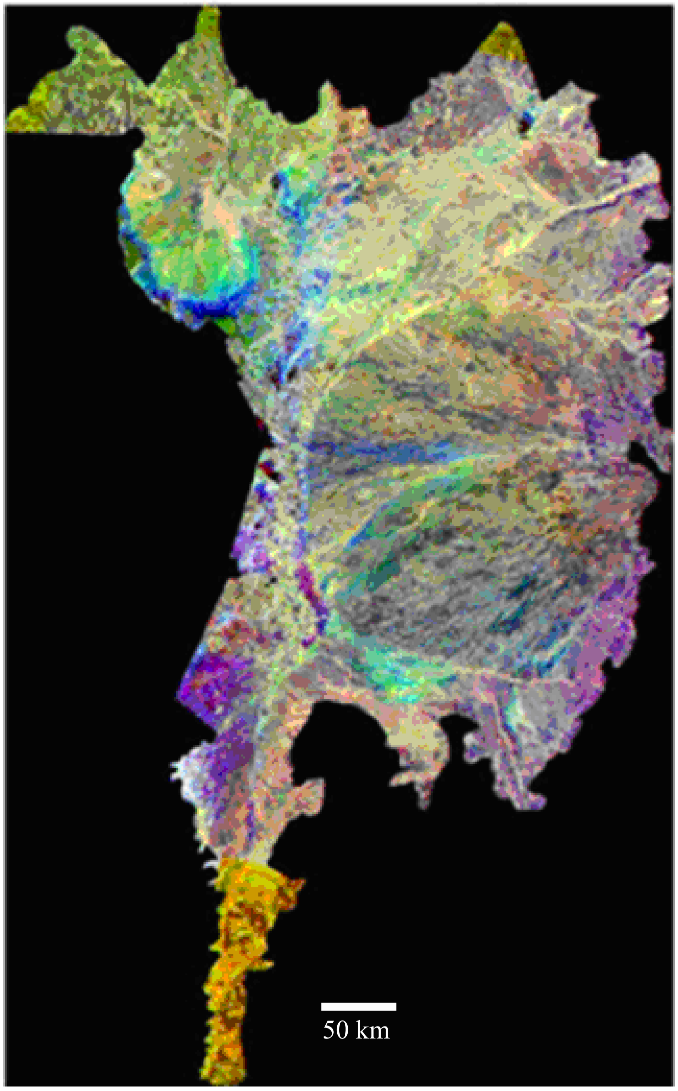

Figure 3: February (R), July (G), Radarsat HV(B) (Note: the lack of blue in the Nabileque subregion is due to the lack of C-band coverage for this area) © *JAXA/METI.*

B: The resulting objects from step A were then subjected to spectral difference segmentation with a factor of 10. This essentially merged any contiguous objects with a spectral difference of <=10 in all 3 layers, thereby reducing the overall number of objects while losing the minimal amount of spectral information. Backscattering values were recorded for the resulting objects over areas of known cover based on ground truth, a priori knowledge of SAR backscattering characteristics, secondary information regarding landscape and flood extent gathered from local inhabitants of area, and examination of high spatial resolution optical imagery (IKONOS and ANVIR-2). These backscattering values were then compared to those gathered from the previously defined ROI (Steps 5 and 6), and rules based on radiometric ranges for classes were formed.

The Level 1 classification encompassed five categories, examples of which can be seen in Figure 4:

- Gallery forest/savanna forest: includes riparian forests on high banks of major rivers, all forests subject to seasonal flooding, and non-floodable forest (cordilheiras and capoes)

- Dense savanna/open savanna: includes areas that are comprised of any combination of shrubs, short trees, herbaceous fields, fields with sparse density trees; may or may not be subject to flooding

- Grasslands/pasture – includes natural grasslands, pastures, agriculture, cultivated fields and farmland; may or may not be subject to flooding. Due to the relative inseparability of the grasslands and pasture classes they were grouped together in one class to avoid confusion

- Herbaceous savanna – includes areas of sandy soils, alluvial fans, floating emergent aquatic vegetation, herbaceous vegetation, waterways, vazantes; subject to seasonal or permanent flooding

- Open water – includes all permanent lakes and rivers

In addition, object area parameters were utilized to separate small freshwater lakes from spectrally similar herbaceous savanna.

Level 2 - Defining Seasonal Change Classification

Numerous studies utilize temporal change in backscattering characteristics of cover types to determine inundation (Martinez & Le Toan 2007; Hamilton et al 2004; Costa 2004; Hess et al 1995; Wang et al 1995). Essentially, areas subject to inundation show seasonal change in backscattering values; areas with no temporal change do not flood and therefore minimum backscattering change was observed. In light of this, algorithms designed to exploit the temporal variability in backscattering were applied to the images (Silva 2009). The first was a cumulative mean distribution algorithm designed to show areas of cumulative change over the entire year:

$$[(a-b)^2 + (a-c)^2 + (a-d)^2 + (a-e)^2 + (b-c)^2 + (b-d)^2 + (b-e)^2 + (c-d)^2 + (c-e)^2 + (d-e)^2]^{0.5}$$

Where,

a = January ALOS image

b = February ALOS image

c = May ALOS image

d = July ALOS image

e = November ALOS image

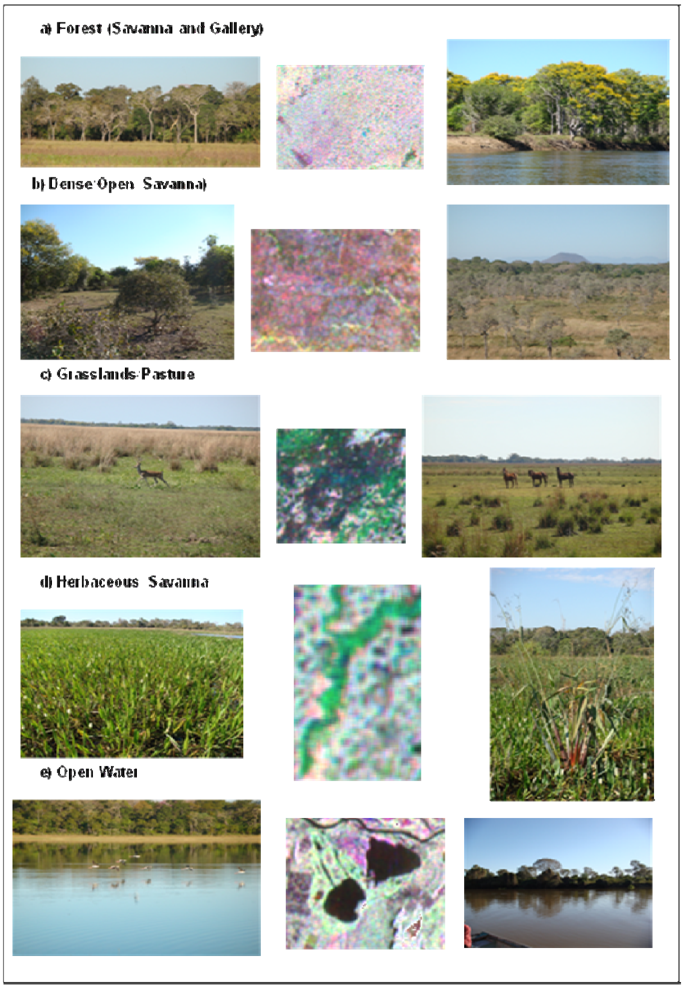

Figure 4 – Examples of Level 1 classification cover types and how they appear in the SAR colour composite Feb-red; Jul-green, Nov-blue.

Individual calculations were performed to show change between each time period.

$[(a-b)^2]^{0.5}$; $[(b-c)^2]^{0.5}$; $[(c-d)^2]^{0.5}$; $[(d-e)^2]^{0.5}$; $[(e-a)^2]^{0.5}$

Applying these algorithms resulted in outputs maps that clearly showed the areas of the most change in backscattering values within these temporal periods. Then, rules based on backscattering were applied to Level 1 Savanna Forest/Gallery Forest and Grasslands/Pasture classes to separate flooded from non-flooded areas.

III. Results and Summary

A. Backscattering Analysis

Sites used for the backscattering analysis (Figure 5) were taken from the Nhecolandia, Aquidauana and Miranda subregions, where field data was gathered. Therefore, any analysis regarding the seasonality of flood patterns is mostly applicable to these areas as other regions in the Pantanal have different flood patterns. However, it is expected that the backscattering signal behaves similarly for the other regions.

Figure 5 – Cross-temporal, multi-sensor comparison of mean backscattering values from training site classes.

(i) Forest (Figure 4a)

Forested areas exhibited the highest backscattering values of all the classes in L-band, for all seasons. Mean values during maximum flood in February ranged from –3.9dB for floodable forest to –8.1dB for non-floodable forest, and mean values during the dry season in July ranged from –6.0 for floodable forest to –7.1 for non-floodable forest. This is the result of multiple scattering mechanisms and interactions with the various components present in forested regions as suggested by Wang et al (1995):

$$\sigma°_t = \sigma°_s + \sigma°_c + \sigma°_m + \sigma°_d$$

where,

$\sigma°_s$ = backscattering from the canopy surface directly back to the sensor

$\sigma°_c$ = volume scattering within the canopy

$\sigma°_m$ = multiple interactions of the canopy and the ground

$\sigma°_d$ = double-bounce scattering

At the long wavelength of L-band, the leaves of the canopy are quasi-transparent, thus the radiation penetrates through to interact with branches, trunks and the underlying surface. The combination of all of these components results in a higher backscattering return than other cover types. However, forested backscattering values are lower in C-band than in L-band as $\sigma°_t$ is almost exclusively made up of $\sigma°_c$, particularly with cross-polarized (HV) C-band as suggested in Wang et al, (1995). Townsend (2002) found that C-band HH polarized radiation may penetrate the canopy structure allowing detection of inundation in forested areas; however in non-flooded conditions total C-band HH backscatter is predominantly due to volume scattering (Wang et al 1995; Townsend 2002). Our C-band data was acquired in August during the dry season, even if some of the radiation did penetrate the canopy there was no water available to cause double-bounce, therefore, C-band HH and HV exhibited only marginal differences for the two forest classes.

Overall mean backscattering values (-5.7dB to –8.1dB for non-floodable forest, and –3.9dB to –6.4dB for floodable forest) were within the expected range for that cover type (Hess et al 1995; Wang et al 1995; Costa 2004; Martinez & le Toan 2007). There was very little variability between ROI values within both of the forest classes (Figure 13). This is likely because large homogenous areas of forest were clearly visible in the data, thus there was less chance of accidentally including pixels that were not representative of the class.

Temporally, L-band signal from non-floodable forest and floodable forest showed little variation between them for May, July, November and January, but a great difference in February. This is because high water occurs in the Nhecolandia region (where the majority of the forest ROI's were located) in February, thus there was increased backscattering for floodable forest attributable to the $\sigma°_d$ component not present in the non-floodable forest class. Floodable forest exhibited slightly higher mean values in L-band than non-floodable forest (0.9dB, 4.9dB, 1.1dB, 0.6dB for Jan, Feb, Jul, and Nov, respectively) for all months except for May, where non-floodable forest was slightly higher than floodable forest (-5.7dB compared to –6.1dB). Although the variation was slight, they could be attributable to differences in tree species. Hess et al (1990) suggested that the relationship between hydrology and tree species must be kept in mind to ensure that observed backscattering differences are the result of flooded/non-flooded conditions and not due to differences in vegetation species.

(ii) Dense/Open Savanna (Figure 4b)

This class covered a wide range of landscapes from open grassy savanna with sparse trees and areas of bare soil to relatively dense areas of herbaceous vegetation, shrubs, and small trees. This diversity of the land cover resulted in the high degree of backscattering variability between sites. Also, the heterogeneous nature of mixed savanna and the relatively low spatial resolution of the data hindered the selection of pure training sites. As such, areas of open grassy savannas exhibit backscattering characteristics closer to grasslands, while dense savannas are more similar to forest.

Generally, floodable dense/open savanna exhibited consistently higher backscattering values than non-floodable dense/open savanna, regardless of the season. Furthermore, values for floodable areas did not change significantly, nor did values for non-floodable areas, regardless of season. The explanation for the differences between the two classes is likely due to different tree and vegetation species inhabiting floodable and non-floodable areas, however, the lack of temporal change is not as easy to clarify. The only possibility speculated upon lies in the nature of the backscattering characteristics of the components present in a savanna landscape; during flooded conditions, the presence of water would cause much of the signal to be specularly reflected away from the sensor, but, the presence of trees and shrubs would add an enhanced double-bounce signal. In a pixel representing $100m^2$ of savanna terrain, these two components could cancel each other out, thereby showing no discernable change between flooded and non-flooded conditions. However, this theory is speculative given the lack of literature pertaining to SAR analysis of areas of mixed terrain such as this in relation to flood detection.

Mean C-band HH and HV backscattering values both fall somewhere in between grasslands/pasture and forest classes (-8.7dB and –14.6dB for HH and HV Dense/Open Savanna, and –7.8dB and –14.6dB for HH and HV Floodable Dense/Open Savanna). This is again to be expected due to the mixed nature of the class.

(iii) Grasslands/Pasture (Figure 4c)

Due to the relative inseparability of the grasslands and pasture classes, these classes are considered together in this analysis. This class represents a variety of herbaceous, grass-like vegetation including: very short grass found around the *vazantes*; croplands of various species; cultivated fields of *Brachiaria sp*. (a hardy introduced plant species used for cattle pasture); and the very tall (~2m) wild grass found on the *campos*.

Overall, the backscattering values for grasslands and pasture, floodable and non-floodable, fell within expected values (Hess et al 1995; Hill et al 1999). The grasslands/pasture class, whether floodable or not, were found to exhibit consistently higher values at C-band HH (mean value of –10.7dB) than at L-band (11.8dB for May, the highest backscattering of the L-band imagery) due to volume scattering interactions with the vegetation. This type of vegetation is usually partially transparent to L-band, however can occasionally exhibit higher values depending on the height and density present. For example, Hill et al (1999) found that thick, lush, ungrazed herbaceous pastures had a backscattering value of –8.8dB in L-band (which is almost comparable to non-floodable forest, and not typical for grasslands). Of the 15 classes of grass tested by Hill et al (1999), the backscattering values exhibited wide divergence from –8.8dB to –23.1 dB in L-band, –5.9dB to –14.5dB for C-band HH, and –6.2dB to –13.5dB for C-band HV; this helps to explain the high variability between grasslands training sites for all our images.

Floodable grasslands and pasture showed lower mean values in January (-15.2dB) and May (-12.5dB), and far lowers values in February (-19.6) than non-floodable areas (-12.8dB, -11.1dB and –13.9dB, respectively). This is consistent with expected results as maximum flood in the region occurs in February, with rising water occurring in January and falling water in May. Low values for this class during inundation are due to increased specular reflection away from the sensor caused by the water surface. Land submergence in the

Pantanal is typically 0.5-1.5m, while the pasture and grasslands training sites covered areas from very short grass (< 0.05m) to very tall (~ 2.0 m). Therefore, flooded areas would show differing degrees of backscattering depending on whether the vegetation (grass) was fully submerged or only slightly flooded. Fully submerged areas would demonstrate a very low backscattering return, as most of the incident radiation would be specularly reflected away from the sensor. However, areas of very tall and/or very dense grass, only slightly flooded (maybe only a few centimetres) would not show as great a degree of difference between flooded and non-flooded as less of the signal would be reflected away, and more would be volumetrically scattered within the vegetation. There was a noticeable difference between C-band floodable and non-floodable pasture, for both HH (-13.0dB for floodable and –8.0dB for non-floodable) and HV (-20.2dB for floodable and –14.9dB for non-floodable) polarizations, which could only be explained by different vegetation species inhabiting the two cover types. The C-band data was acquired in August during the dry season, therefore no difference in backscattering could be attributable to actual flood conditions. Another phenomenon found in the data was the seemingly inconsistent pattern of backscattering present in the non-floodable area: high values in May and November but low in July. One possible explanation for this may be the changing dielectric properties of the vegetation (Dobson et al 1996). Although these are not floodable areas they are still susceptible to climate. July is in the middle of the dry season and the lack of precipitation, along with senescence of the vegetation, results in a lowering of the moisture content, and hence the backscattering value. May is at the end of the rainy season and November at the beginning, therefore the vegetation would like contain a greater moisture content than in July.

(iv) Herbaceous Savanna (Figure 4d)

This class encompasses herbaceous aquatic/amphibious vegetation occurring on alluvial fans, *vazantes* and waterways. The lowest L-band values for this class occurred in February (-21.2dB), during maximum flood in this region. At this time, any vegetation present is likely to be fully submerged, or of the small free-floating broadleaf variety (3-30cm in height). Therefore, the majority of L-band radiation would be specularly reflected away from the sensor, resulting in the low backscattering return. The highest L-band values were found in July (-9.8dB), during low water. At this time, a possible new group of herbaceous vegetation adapted to the drier conditions would be present, thereby increasing the backscattering return. For example, rooted forms of broad-leafed aquatic vegetation would have more ability to take hold and thrive in less turbulent low waters than in the relatively faster moving, deeper waters occurring during maximum flood. Also, more Aquatic Terrestrial Transition Zone (ATTZ) amphibious vegetation becomes exposed with receding waters further increasing the backscattering signal. This further explains the high variability in January and May as differing degrees of water level would be present depending on localized flood conditions.

C-band HH values were high (-8.6dB) compared to L-band for this class, as less of the vegetation is interacting with L-band due to the longer wavelength. The C-band imagery was acquired in August, therefore more vegetation would be exposed, increasing the degree of volume scattering and decreasing the degree of specular reflection. The backscattering of aquatic vegetation at C-band is primarily through volume scattering, although double-bounce scattering has been observed with dense, tall (~1m) aquatic vegetation (Hess et al 1995; Costa 2004, Martinez & le Toan 2007).

(v) Open Water (Figure 4e)

The open water class was expected to show consistently low values in both C-band and L-band (-18.3dB, -20.6dB, -16.9dB, -20.1dB, -20.2dB, -20.0dB and –26.3dB for L-band Jan, Feb, May, Jul, Nov, and C-band HH and HV, respectively), as the majority of the incident radiation would be specularly reflected away from the sensor. For example, Martinez & le Toan (2007) reported open water in the Amazon floodplain to have values of –17.0 dB with a negligible variation of +/-0.3dB in L-band. However, the open water training sites for this study showed slightly elevated values in May and February for L-band, and fairly high variability between training site values. One possible explanation for the variability is the presence of migrating floating *camalotes* of aquatic vegetation, which, if tall enough, and dense enough, could cause some volumetric scattering increasing the signal to the sensor from individual training sites. Another explanation could be an increase in water surface roughness caused by wind (Oliver & Quegan 2004).

B. Separability between classes

The best separability between flooded and non-flooded classes occurred in February (Figure 6). This is to be expected, as February is the high water season for the area, and would thus show the most variability between flooded and non-flooded areas. The overlap in backscattering values between forest classes, savanna classes and grasslands/pasture classes was anticipated due to the fuzzy borders between them. Dense/open savanna is a class that bridges forest and grasslands, and therefore contains varying degrees of both cover types. Although herbaceous savanna and open water were virtually indistinguishable in February during maximum inundation, they were easily separated in July. This is because lowering water levels resulted in the exposure of more vegetation cover for herbaceous savanna, thereby increasing the backscattering signal, especially in C-band, while backscattering for open water remained fairly low. The high degree of overlap between floodable and non-floodable grasslands and pastures is due to the similar nature of the two classes. They both represent areas of low vegetation devoid of trees, however height and density of both classes is variable, so they are easily confused.

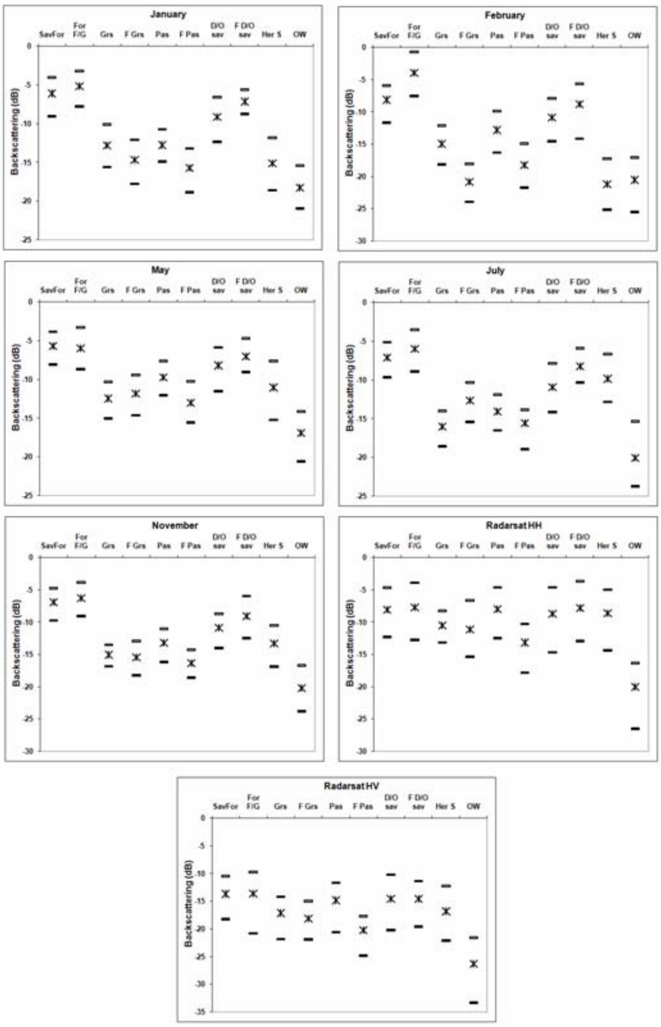

Figure 6 – Variability between classes: Savanna Forest, Forest Floodable/Gallery, Grasslands, Floodable Grasslands, Pasture, Floodable Pasture, Dense/Open Savanna, Floodable Dense/Open Savanna, Herbaceous Savanna, Open Water.

C. Level 1 Classification

The Level 1 classification map is shown in Figure 7. A classification accuracy assessment was performed on the Level 1 classification using the ROI's defined in Step 5. The confusion matrix (Table 2) shows that open water and herbaceous savanna were 100% correctly classified in Definiens. For forest, 76% were correctly classified, while 14% were misclassified as dense/open savanna. As predicted by the backscattering analysis in the previous section, there was a high degree of uncertainty between grasslands/pasture and herbaceous savanna; only 58% of grasslands/pasture was correctly classified, while 38% was classified as herbaceous vegetation and 3 % as dense/open savanna. Also as predicted, there was a considerable overlap between forest, dense/open savanna and grasslands/pasture; 50% were correctly classified while 25% were misclassified as forest and 25% were misclassified as grasslands pasture.

Large areas of aquatic macrophytes (herbaceous savanna) were observed in the data when examining the optical images. These areas were not included in the original backscattering analysis, as there was no ground truth to validate them. However, a high degree of confusion was present between forest and these large areas of herbaceous vegetation. Rules were created to separate the two classes and a visual comparison of the entire image with the optical data showed an improvement. Confusion between aquatic macrophytes and forest classes in L-band has been reported in several cases (Hess et al 1990; Hess et al 1995; Pope et al 1997). Our data exhibited high backscattering values for large areas of aquatic macrophytes similar to values found in the forest classes. Pope et al (1997) reported that L-band double-bounce interactions were possible for herbaceous aquatic vegetation at relatively steep incidence angles (25° at swath center for their study). Therefore, this could explain the high values for our study as the L-band imagery was acquired at a relatively steep incidence angle of 27.1°. Hess et al suggested that forest and macrophytes were best separated at L-band HV polarization (1995), or with a range of different incidence angles (1990). After a great degree of manual comparison of values for areas of aquatic macrophytes and forest, the greatest degree of separability between the two was found to be between the November L-band and the C-band HH imagery; thus a rule exploiting this difference was created to separate the two in the Level 1 classification. Also, areas of upland hills were misclassified due to increased elevation and shadow effects; these areas were corrected manually.

Overall, the confusion found between classes in the Definiens classification were consistent with the results established in the backscattering analysis. However, the ROI's, and resultant accuracy assessment, are only representative of the field study subregions of Nhecolandia, Aquidauana/Negro and Miranda. Due to the variable nature of the Pantanal floodplain as a whole, the same level of confidence cannot be transferred to the entire study area; however we intend to improve the accuracy of the classification during the Phase 2 of this project, where other areas of the Pantanal will be visited.

D. Level 2 Classification

The temporal series of mosaic images representing the separation between flooded forest and non-flooded forest can be seen in Figure 8. For the most part, areas representing flooded forest for the majority of the time follow riparian corridors, except for the large northern area spanning parts of the Piquiri/Sao Lourenco, Cuiaba and north Paraguay subregions mentioned previously. Areas of forest that never flood are present in all subregions, but are particularly apparent in the Nhecolandia, Taquiri Fan, and Corixo Grande subregions. The mapped flood timing is consistent with that reported in Hamilton et al (1996) and the hydrological data shown in Figure 2. For example, rising water in January and maximum flood in February have been reported for the Piquiri/Sao Lourenco, Nhecolandia, and Aquidauana/Negro subregions, and this can be seen by the darker green, representing flooded forest, along the riparian areas of these three subregions for the January and February images.

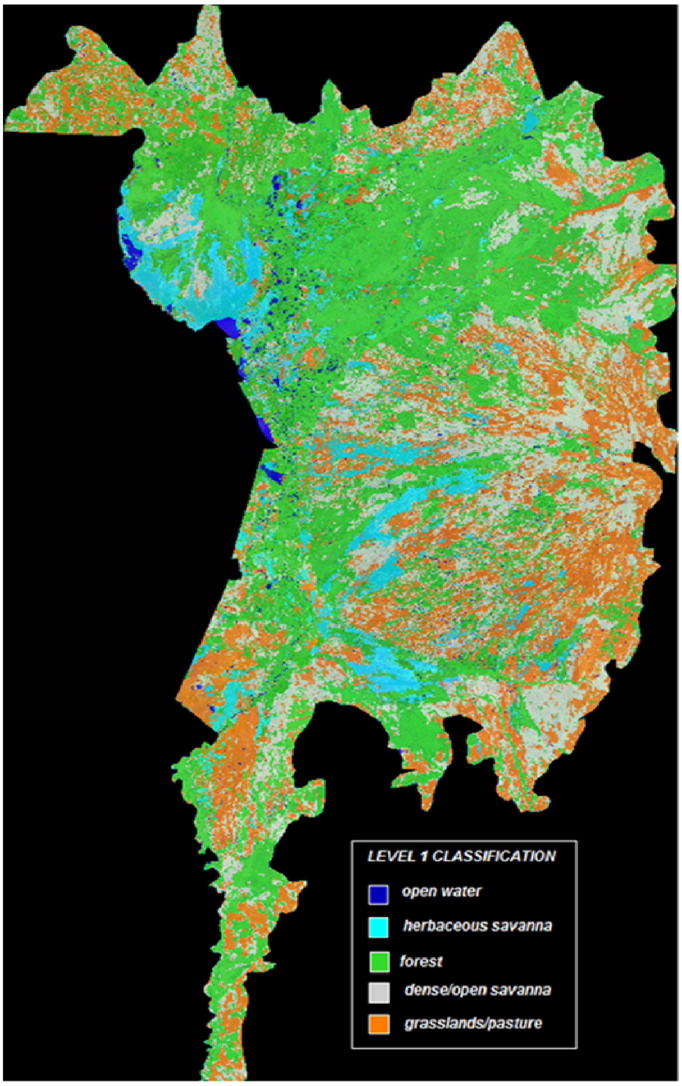

Figure 6.2 – Level 1 classification output

Figure 7 – Level 1 Classification output. ALOS K&C © *JAXA/METI.*

Table 2. Level 1 confusion matrix.

Confusion Matrix for Level 1 Classification of the Brazilian Floodplain					
	Gallery/Savanna Forest	Dense/Open Savanna	Grasslands/Pasture	Herbaceous Savanna	Open Water
Gallery/Savanna Forest	13	4	0	0	0
Dense/Open Savanna	3	6	3	0	0
Grasslands/Pasture	0	1	17	11	1
Herbaceous Savanna	0	0	0	9	0
Open Water	0	0	0	0	4

However, the dark green begins to recede and is replaced by the light green, representing non-flooded forest, in May, and particularly in July and November for these regions. Conversely, the lower Paraguay River shows more dark green (flooded forest) in July than in February, which is consistent with the timing of maximum flood found in that subregion. We speculate that some areas of flooded forest not in agreement with the reported flooding regime for each of the subregions may be a result of the confusion between aquatic macrophytes and forest reported previously; the methods employed for separating the two classes were experimental, and therefore may not have done an adequate job. The Nabileque subregion shows flooded forest in all months except for July, contrary to GEF (2004), which reports localized flooding only along the Paraguay River itself, and to Hamilton et al (1996) who report the greatest degree of flooding in this region in July. Therefore we suggest that perhaps the species of forest in this region show higher backscattering values than other forest regions and thus fell within the range designated for flooded forest and was erroneously classified. The Nhecolandia region shows very little flooding with the forest class throughout the year indicating a high degree of savanna forest made up of *capoes* and *cordilheiras*, which is consistent with what was observed in the area during the field campaign.

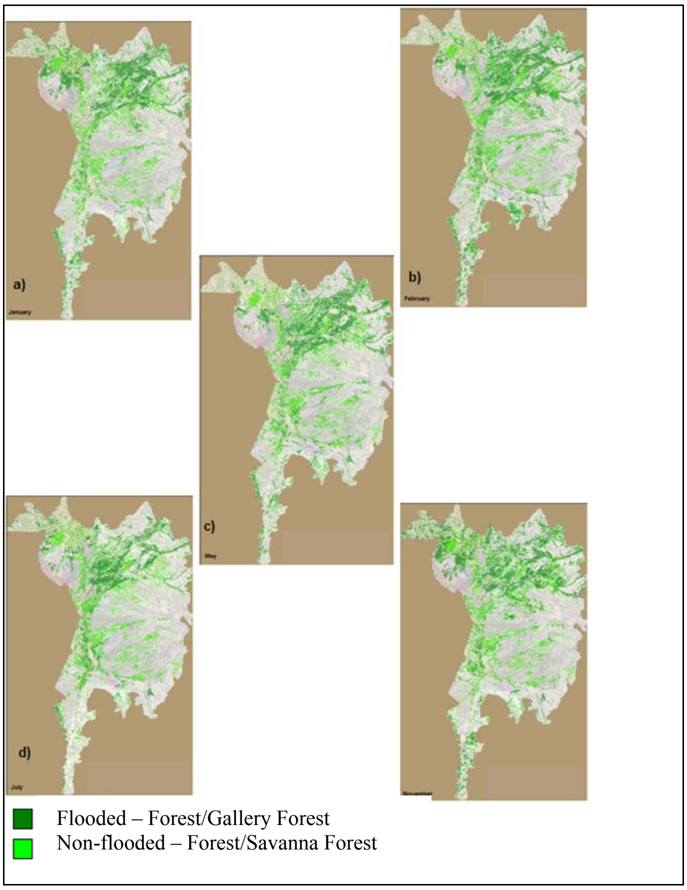

Figure 8 – Level 2 Classification output. Flooded Forest vs. Non-Flooded Forest for: a) January; b) February; c) May; d) July; e) November . ALOS K&C © *JAXA/METI.*

The temporal series of mosaic images representing the separation between flooded and non-flooded grasslands/pasture can be seen in Figure 9. Overall, the areas representing flooded grasslands are very low compared to non-flooded, however there are some notable results. The January image shows small areas of flooding in the Nhecolandia and Taquiri Fan subregions, greatly increasing in the February image. Both January and February show small areas of flooding in localized patches of the northern Paraguay and northern Nabileque subregions as well. The area of the greatest observable flooding occurs in the Nhecolandia region in February, and in the southern Paraguay River subregion in July, consistent with observed results in Hamilton et al (1996) and the maximum river discharge timing seen in Figure 2. May shows very little flooding anywhere except for the Corixo Grande subregion, and localized portions of the Paraguay. Flooded areas are apparent in the southern Paraguay/northern Nabileque subregions for July, as well localized areas in the east of the entire mosaic. November shows no flooded areas anywhere except for small areas in the southeast Taquiri Fan and east Nhecolandia.

V. CONCLUSIONS

Examination of the SAR ALOAS/PALSAR and RADARSAT-2 data used for this study, coupled with data gathered in the field, provided an understanding of the interactions between incident microwave radiation at L and C bands and ground cover, and how they change temporally with the seasonal flood in the Brazilian Pantanal. In general, the Definiens object-based Level 1 classification using both bands yield an average accuracy of 77%, in which the most confusion was between grassland/pasture and herbaceous and open savanna classes. This was expected given (1) the nature of these landscape covers, i.e., mostly grass-like vegetation and (2) the 100 m course resolution of the ScanSAR imagery. Nonetheless, our work provided the most detail classification of landscape cover available for the entire Brazilian Pantanal.

The generated flooded/non-flooded maps provided consistent separation of flooded from non-flooded forest. However, as expected due to similar backscattering values at this spatial resolution, L-band HH was not ideal for separating flooded from non-flooded grasslands/pasture, or flooded from non-flooded dense/open savanna. Nonetheless, much of the temporal pattern of inundation defined the classified maps was consistent with that found in Hamilton et al (1996), with some areas of disagreement. However, Hamilton et al (1996) used passive microwave data and did not provide an accuracy assessment or temporal output maps to validate their study. As such, we can not truly compare our spatial maps with their results.

Generally, two main factors contributed to confusion and erroneous classification in the Definiens software. First, low spatial resolution (100m), further degraded by the SAR speckle filtering process, may have led to a high degree of mixing of cover types with segmented image objects. The Pantanal is a highly heterogenous landscape where a single pixel representing $10000m^2$ often contains forest, grasslands, and lake elements within the same pixel.

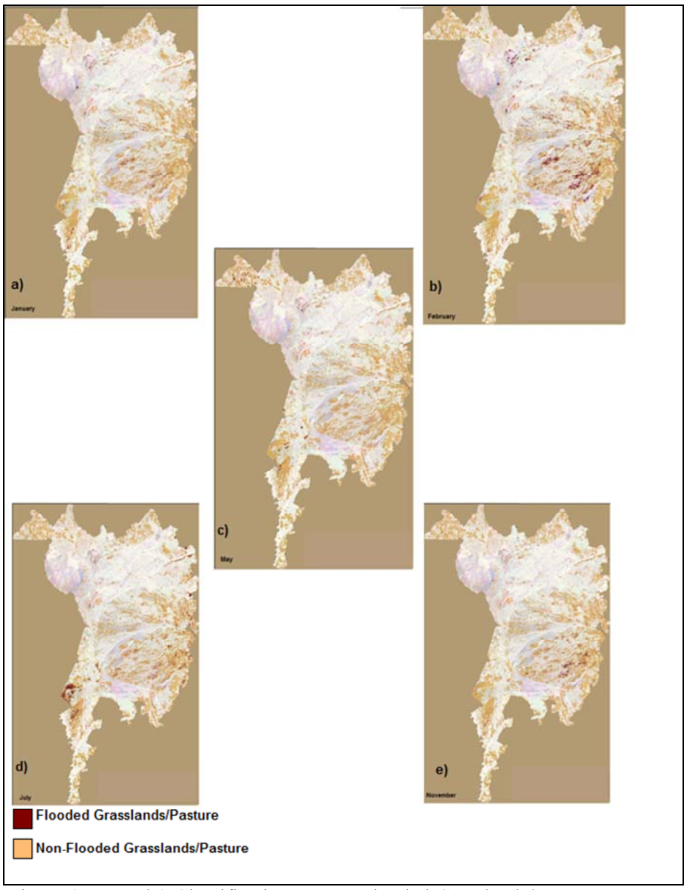

Figure 9 – Level 2 Classification output. Flooded Grasslands/Pasture vs. Non-Flooded Grasslands/Pasture for: a) January; b) February; c) May; d) July; e) November. ALOS K&C © *JAXA/METI.*

Second, varying seasonal flood regimes for the many different subregions in the Pantanal increased the difficulty in selecting rules for determining separation between classes. Interpolating what we knew to be true in the area where we had conducted field work to the rest of this complex wetland system was problematic because the timing of the flood was different for different subregions, and there were areas where ground cover information was not available.

Improvements on both land-cover and temporal flooding classifications will come by (1) splitting the Pantanal mosaic into hydrological subregions based on peak river discharge, and conducting separate classifications for each area. (2) The addition of a temporal series of C-band data corresponding to a time series of L-band, and (3) field data acquired in the wet season. Further improvement will come from the analysis of 12.5 m fine resolution mosaics of the second phase of this project and planned field work in the northern and central Pantanal.

In conclusion, utilizing multi-temporal, multi-band SAR data for defining land cover and inundation patterns in the Pantanal was accomplished. The delineation of the landcover will be used as input spatial data in future studies involving land use or habitat monitoring (part of our collaboration with EMBRAPA-

Brazil in the phase 2 project). Although there have been several previous habitat studies at a local scale in the Pantanal (Tomas et al, 2001), only a few have covered the entire Pantanal at a regional scale (Hamilton et al, 1996; but does not provide spatial maps), as the size and relative inaccessibility of the region hinders traditional methods of data collection. Ultimately, the generated data from phase 1 and 2 will aid in further understanding the spatial and temporal pattern of the flood-pulse regime in the Pantanal, and will provide seasonal habitat suitable for threatened species, and define corridors and connectivity for defining conservation areas.

ACKNOWLEDGEMENTS

This work has been undertaken within the framework of the JAXA Kyoto & Carbon Initiative. ALOS PALSAR data have been provided by JAXA EORC. The authors would like to acknowledge the K&C group for the interesting fun meetings and valuable technical information learned from this team. In special, we thank you A. Rosenqvist, M. Shimada, and M. Watanabe for all the effort and patience with us during all these years. Special thank you to JAXA for partially support all the K&C projects; it is invaluable! Thank you to the Canadian Space Agency for providing Radarsat-2 imagery under the SOAR program. Many thanks to The National Geographic Society for funds for field work.

REFERENCES

[1] Abdon M, da Silva J, Pott V J, Pott A, da Silva M P. (1998). Utilization of analogic data of Landsat-TM on screening vegetation of part of the Nhecolandia subregion of the Brazilian Pantanal. Brazilian Journal of Agricultural Research. 33:1799-1813.

[2] Costa M P F, Telmer K H. (2007). Mapping and monitoring lakes in the Brazilian Pantanal wetland using synthetic aperture radar imagery. Aquatic Conservation: Marine and Freshwater Ecosystems. 17: 277-288.

[3] Costa M P F, Telmer K H. (2006). Utilizing SAR imagery and aquatic vegetation to map the fresh and brackish lakes in the Brazilian Pantanal. Remote Sensing of the Environment. 105: 204-213.

[4] Costa M P F. (2004). Use of SAR satellites for mapping zonation of vegetation communities in the Amazon floodplain. International Journal of Remote Sensing. 25(10): 1817-1835.

[5] Costa M P F, Niemann O, Novo E, Ahern F, Mantovani J. (2002). Biophysical properties and mapping of aquatic vegetation during the hydrological cycle of the Amazon floodplain using JERS-1 and Radarsat. International Journal of Remote Sensing. 23 (7): 1401- 1426.

[6] da Silva C J, Girard P. (2004). New challenges in the management of the Brazilian Pantanal and catchment area. Wetlands Ecology and Management. 12:533-561.

[7] Dobson M C, Pierce L E, Ulaby F T. (1996). Knowledge based land cover classification using ERS-1/JERS-1 SAR composites. IEEE Transaction of Geoscience and Remote Sensing. 34(1): 83-99.

[8] GEF (Global Environment Facility) Pantanal/Upper Paraguay Project. (2004). Implementation of Integrated River Basin Management Practices in the Pantanal and Upper Paraguay River Basin. Strategic Action Program for the Integrated Management of the Pantanal and Upper Paraguay River Basin. ANA/GEF/UNEP/OAS. Brasilia: TDA Desenho & Arte Ltda. 2004.

[9] Gottgens, J. F., R. H. Fortney, J. Meyer, J. E. Perry, and B. E. Rood. 1998. The case of the Paraguay-Parana´ waterway (‘‘Hidrovia’’) and its impact on the Pantanal of Brazil: a summary report to the Society of Wetlands Scientists. Wetlands Bulletin:12–18.

[10] Hamilton, S. K., S. J. Sippel, and J. M. Melack. (1996). Inundation patterns in the Pantanal wetland of South America determined from passive microwave remote sensing, Arch. Hydrobiol., 137, 1 – 23, 1996.

[11] Hamilton, S. K. (1999). Potential effects of a major navigation project (the Paraguay–Parana Hidrovıa) on inundation in the Pantanal floodplains. Reg. Rivers Res. Manage. 15: 289– 299.

[12] Hamilton S K. (2002). Human impacts on hydrology in the Pantanal wetland of South America. Water Science and Technology. 45(11): 35-44.

[13] Hamilton, S. K., S. J. Sippel, and J. M. Melack. (2004). Seasonal inundation patterns in two large savanna floodplains of South America: The Llanos de Moxos (Bolivia) and the Llanos del Orinoco (Venezuela and Colombia). Hydrological Processes. 18: 2103-2116.

[14] Heckman, C. W. 1998. The Pantanal of Poconé: Biota and ecology in the northern section of the world’s largest pristine wetland. Kluwer Academic Publishers, The Netherlands.

[15] Hess L L, Melack J M, Filoso S, Wang Y. (1995). Delineation of inundated area and vegetation along the Amazon floodplain with the SIR-C synthetic aperture radar. IEEE Transactions on Geoscience Remote Sensing. 33: 896-904

[16] Hill M J, Donald G E, Vickery P J. (1999). Relating radar backscatter to biophysical properties of temperate perennial grassland. Remote Sensing of the Environment. 67:15-31.

[17] JAXA – Japanese Aerospace Exploration Agency. (2009). Advanced Land Observing Satellite. Internet Resource Accessed January 20 2009. http://www.jaxa.jp/projects/sat/alos/index_e.html

[18] Junk W J, da Cunha C N, Wantzen K M. (2006). Biodiversity and its conservation in the Pantanal of Mato Grosso, Brazil. Aquatic Sciences. 68(3): 278-309.

[19] Le Toan T, Ribbes F, Wand L, Floury N, Ding K, Kong J A, Fujita M. (1997). Rice crop mapping and monitoring using ERS-1 data based on experiment and modeling results. IEEE Transactions on Geoscience and Remote Sensing 35: 41-55.

[20] Martinez J M, le Toan T. (2007). Mapping of flood dynamics and spatial distribution of vegetation in the Amazon floodplain using multitemporal SAR data. Remote Sensing of the Environment. 108: 209-223.

[21] MacDonald, Dettwiler and Associates Ltd.13800 Commerce Parkway. Richmond, British Columbia, Canada V6V 2J3.

[22] Oliver C, Quegan S. (2004). Understanding synthetic aperture radar images. SciTech Publishing, Inc. Raleigh, NC.

[23] Pope K O, Rejmankova E, Paris J F, Woodruff R. (1997). Detecting seasonal flooding cyclesinmarshes of the Yucatan Peninsula with SIR-C polarimetric radar imagery. Remote Sensing of the Environment. 59:157-166.

[24] Por F D. (1995). The Pantanal of Mato Grosso (Brazil): World’s Largest Wetlands. Monographiae Biologicae. Vol 73. Dumont H J & Werger M J A (eds). Kluwer:Dordrecht.

[25] Rosenqvist A, Shimada M, Ito N, Watanabe M. (2007). ALOS PALSAR: A pathfinder mission for global-scale monitoring of the environment. IEEE Transactions on Geoscience and Remote Sensing. 45(11): 3307-3317.

[26] Silva T S F, Costa M P F, Melack J M, Novo E M L M. (2008) Remote sensing of aquatic vegetation: theory and applications. Environmental Monitoring and Assessment. 140(1-3): 131-145.

[27] Townsend P A. (2002). Relationships between forest structure and the detection of flood innundation in forested wetlands using C-band SAR. International Journal of Remote Sensing. 23(3): 443-460.

[28] Wang Y, Hess L L, Solange F, Melack J M. (1994).Canopy penetration studies: modeled radar backscatter from Amazon floodplain forests at C-, L- and P-band. Geoscience and Remote Sensing Symposium. IGARSS. Surface and Atmospheric Remote Sensing: Technologies, Data Analysis and Interpretation. International 2(8-12): 1060 – 1062.

[29] Wessels, J., PCI Geomatics. Personal communication via email, Dec 16 2008.


Maycira Costa and Kevin Telmer, professors at the University of Victoria, Canada, Nattan, 6 years old, and Maiara, one month old. One way or the other they are all part of the K&C project.


Terresa Evans is a student in the Geography Department at UVic. Terri is a key player in this project and will be developing her graduate thesis as part of the second phase of the K&C project - Pantanal.